Materials Science-Poland
Volume 44 Issue 1 · pp. 108–126 · DOI: 10.2478/msp-2026-0007

Materials Science-Poland

Influence of binder-to-sand ratio on mechanical and durability properties of ultra-high-performance concrete reinforced with novel polyoxymethylene fiber

Research Article

Wen-Ten Kuo, Wen-Ling Wang, Sung-Ching Chen*

Department of Civil Engineering, National Kaohsiung University of Science and Technology, No. 415 Jiangong Road, Sanmin District, Kaohsiung City, Taiwan

Received 16 January 2026; Accepted 10 April 2026

Abstract: Ultra-high performance concrete (UHPC) faces cost and shrinkage challenges due to high binder contents. This study systematically investigates the influence of varying binder-to-sand (B/S) ratios (0.8, 0.9, 1.0, and 1.2) coupled with novel polyoxymethylene fibers (POMFs, 0 and 2% dosages) on UHPC properties. A fixed water-to-binder ratio (0.17) and 50% ground granulated blast-furnace slag replacement were used. Freshness, mechanical properties, durability, and microstructural properties were evaluated. Results indicate that the B/S ratio critically governs UHPC performance. Contrary to the assumption that higher binder content is always superior, an optimal balance emerged at a B/S ratio of 0.9. This ratio yielded the highest 28-day compressive and splitting tensile strengths, the lowest water absorption, and exceptional sulfate resistance, with no strength degradation after 180 days. A low B/S ratio (0.8) caused insufficient aggregate coating, increasing porosity, and reducing strength. Conversely, an excessive B/S ratio (1.2) induced severe autogenous shrinkage and microcracking, impairing durability and strength. While a 2% POMF addition provided limited gains in compressive strength, it significantly improved splitting tensile strength and shifted the failure mode from brittle to ductile. Scanning electron microscopy confirmed that POMF's hydrophilic nature ensures excellent interfacial bonding with the matrix. Ultimately, a B/S ratio of 0.9 provides the optimal eco-efficient mix design, balancing high performance with material economy for UHPC engineering applications.

Keywords: *Ultra-high-performance concrete • Binder-to-sand ratio • Polyoxymethylene fiber • Mechanical properties • Durability properties*

1. Introduction

1.1 Development of ultra-high-performance concrete (UHPC) and sustainability challenges

UHPC is a novel cementitious composite characterized by ultra-high strength and ductility. Compared to conventional concrete, UHPC exhibits superior compressive and tensile strengths, as well as enhanced resistance to the ingress of harmful substances such as chloride ions, thereby extending the service life of structures and reducing maintenance costs. Bajaber and Hakeem [1] reviewed the evolution of UHPC and highlighted its vast potential for use in modern construction to build more resilient infrastructure. The fundamental design concepts of UHPC focus on improving microstructure and enhancing toughness. Yoo and Banthia [2] demonstrated that the mechanical properties of such cementitious composites heavily rely on optimal fiber reinforcement. Xu et al. [3] indicated that specific curing regimes directly dictate the initial microstructural formation and the development of concrete strength. Yoo et al. [4] observed that incorporating nanomaterials refines the matrix and reduces intrinsic micro-defects. Shi et al. [5] established that optimizing

* *E-mail: jaosn314@nkust.edu.tw*

Open Access. © 2026 the author(s), published by Wroclaw University of Science and Technology
This work is licensed under the Creative Commons Attribution-NonCommercial-NoDerivs 4.0 License.

raw materials and granular packing is essential to reduce intrinsic porosity and improve overall homogeneity. Ghafari et al. [6] further confirmed that using statistical mixture design approaches consistently yields eco-efficient UHPC architectures.

Key strategies for UHPC formulation include incorporating superplasticizers (SPs) and using a low water-to-binder (w/b) ratio of 0.15–0.25. Yu et al. [7] proved that this specific w/b range effectively minimizes unhydrated cement porosity and maximizes matrix density. Sharma et al. [8] detailed how mineral admixtures synergize with this low w/b to dramatically enhance overall particle packing efficiency. Additionally, the inclusion of supplementary materials is vital. Song et al. [9] comprehensively reviewed how supplementary cementitious materials (SCMs) synergize with these dense matrices to enhance long-term durability and mitigate chemical attacks greatly.

However, the early development of UHPC relied on exceptionally high binder contents, with cement usage ranging from 800 to 1,200 kg/m^3, which is nearly three to four times that of traditional concrete. Khan and Yong [10] demonstrated that this excessive cement consumption significantly increases the heat of hydration, creating thermal stresses in mass elements. Bellum et al. [11] noted that such high binder usage imposes significant environmental constraints and increases production costs. Zaki et al. [12] used non-destructive testing to evaluate how modifying these structural configurations affects the corrosion resistance and degradation of eco-friendly mixes. Research has consistently indicated that in UHPC with a low w/b, approximately 30–35% of the cement remains unhydrated, serving merely as a structural filler. Zhang et al. [13] emphasized that the overall unreacted paste volume critically dictates shrinkage behavior and dimensional stability. Consequently, the utilization of industrial by-products as SCMs to replace unhydrated cement has become a key trend. Kim et al. [14] evaluated how replacing cement with high volumes of industrial slags actually improves the flowability and sustainability of dense structures. Wei et al. [15] subsequently modeled how the modified interface bonding in these eco-friendly matrices translates into improved macroscopic tensile behavior.

1.2 Criticality of binder and binder-to-sand (B/S) ratio

Even with partial replacement of cement with SCMs, designs with high binder content still suffer from issues such as high heat of hydration, significant shrinkage, and susceptibility to cracking. Conversely, low binder content may lead to insufficient aggregate coating, resulting in reduced workability and increased porosity. Therefore, the quantity of binder (specifically, the binder-to-aggregate ratio) significantly affects the strength and durability, making the optimization of binder content crucial. Wang et al. [16] pointed out that optimized binder filling directly governs fiber bridging efficiency and tensile stress transfer.

Relevant research confirms that an optimal B/S ratio significantly influences engineering properties. Yao et al. [17] demonstrated that varying the sand-to-binder ratio systematically affects cracking behavior and multiple-cracking characteristics in cementitious composites. Zailani et al. [18] discovered that both excessively high and low B/S ratios are highly detrimental to the structural integrity and compressive strength of repair mortars. Paul and John [19] observed that binder contents exceeding an optimal threshold limit strength gains and cause poor particle distribution. Wahab et al. [20] further demonstrated that modifying the binder composition and aggregate interfaces significantly dictates rheological flowability in self-compacting matrices. These individual studies corroborate that an optimal B/S ratio can improve bond strength and facilitate a favorable interfacial transition zone (ITZ); however, current research remains fragmented and lacks a systematic approach.

1.3 Fiber toughening technology and novel polyoxymethylene fiber (POMF)

Despite UHPC's high strength, its inherent brittleness makes ductility a critical concern. Fibers transfer stress across the matrix and inhibit crack propagation. Zhao et al. [21] confirmed this energy absorption mechanism specifically in synthetic plastic fibers under dynamic compression. Shen et al. [22] observed that introducing fibers actively mitigates early-age autogenous shrinkage and minimizes restrained cracking. Pakravan and Ozbakkaloglu [23] suggested that an optimal dosage of polymer fibers is strictly required to maintain workability while providing structural benefits. Deng et al. [24] confirmed that polymer fibers primarily enhance multi-scale bridging rather than matrix compressive strength. Shen et al. [25] demonstrated that careful spatial distribution of fibers drastically enhances post-cracking flexural performance and toughness.

POMF is a novel high-performance polymer fiber characterized by high strength, impact resistance, chemical resistance, low air entrainment, and excellent dispersion. Zhang et al. [26] characterized its high interfacial bonding

strength with cement composites compared to traditional polymers. Rui et al. [27] found that POMF exhibits excellent ductility and exceptional long-term durability in highly alkaline environments. Lin et al. [28] demonstrated that POMF's hydrophilic nature enables superior dispersion and mitigates balling compared to traditional synthetic fibers. Shen et al. [29] confirmed that POMF is highly effective in reducing tensile creep and autogenous shrinkage in high-performance concrete.

In summary, research on UHPC performance has primarily focused on single variables such as w/b ratio, SCM replacement levels, material types, and fiber content, often utilizing a fixed B/S ratio. The systematic influence of B/S as a variable has been largely overlooked. The innovation of this study lies in addressing the lack of systematic investigation into the interaction between varying B/S ratios and novel polymer fibers (such as POMF), specifically the "coupling effect" on fresh, mechanical, and durability properties. To fill this research gap, this study investigates a detailed range of B/S ratios (0.8–1.2), referencing the typical UHPC mix proportions proposed by ACI Committee 239 [30]. Using cement and ground granulated blast-furnace slag (GGBFS) as binders and silica fume (SF) as a filler for silica sand, this study investigates the impact of varying B/S ratios and the addition of POMF (0 and 2%) on the properties of UHPC. The objective is to identify the optimal B/S equilibrium point that balances mechanical performance and durability.

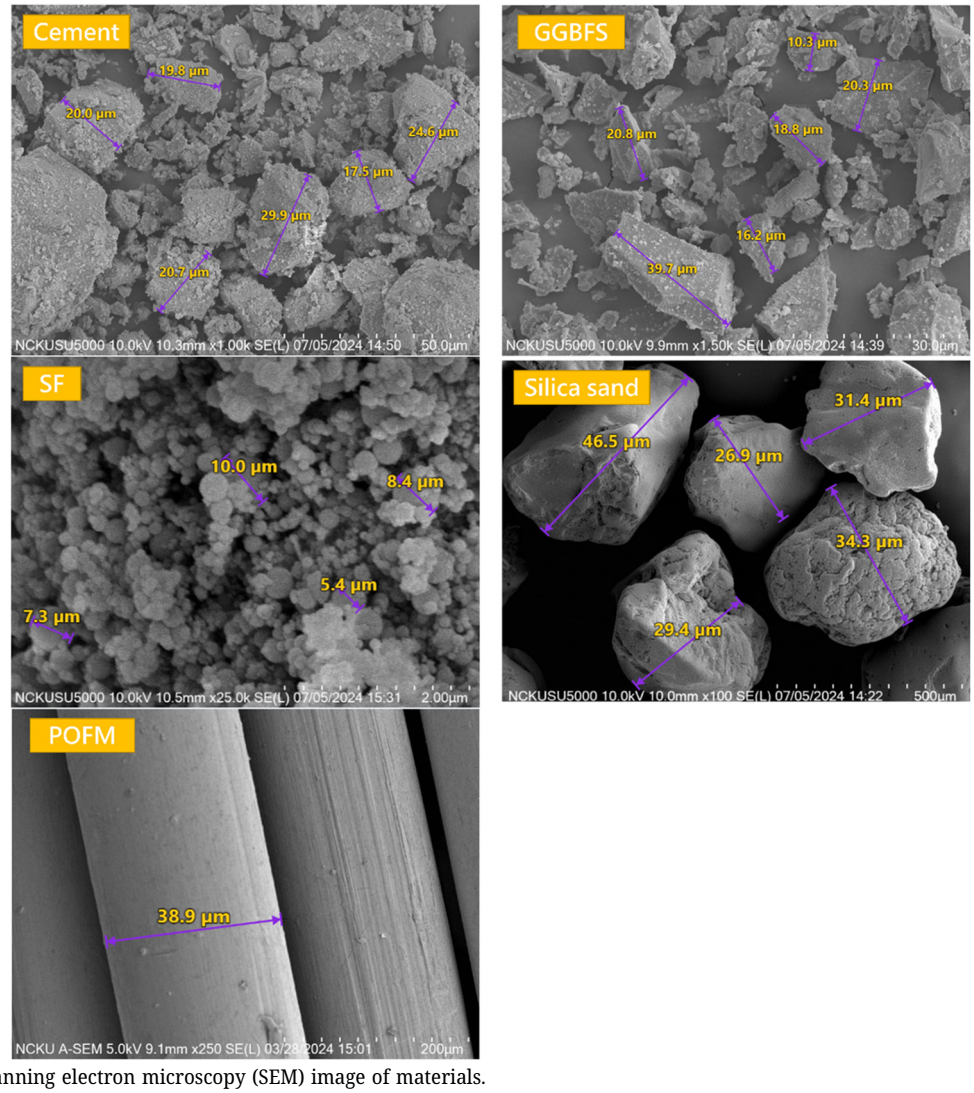


Figure 1. Scanning electron microscopy (SEM) image of materials.

2. Materials and methods

2.1 Material

Type CHIN YU Corporation supplied Portland cement and GGBFS (Grade 100). SF, provided by Sika Taiwan Ltd (Elkem Microsilica 940U), was undensified with a particle size of approximately 0.15 μm. The silica sand, sourced from Vietnam and supplied by Chin Ching Silica Sand Co., Ltd (Model 4V), had a primary particle size range of 150–425 μm. To enhance workability, a polycarboxylate-based SP (GP-401 from Kao Pu Industrial Co., Ltd) with early-strength and slump-retention properties was used. It appeared transparent, with a solid content of 44.7% and a water reduction rate of 32%. To mitigate brittleness, POMFs supplied by Model Technology Corporation were incorporated. These short fibers had a length of 6 mm, a diameter of 0.18 mm, an aspect ratio of 33, and a tensile strength of up to 960 MPa. The microscopic characteristics and physicochemical compositions of these materials are presented in Figure 1 and Tables 1 and 2.

Component	Specific gravity	Specific surface area (m^2/kg)	Specific gravity and absorption of fine aggregates (%)
Cement	3.13	370	—
GGBFS	2.90	460	—
SF	2.21	15,000	—
Silica sand	2.64	—	0.9
POMF	1.41	—	—

Table 2. Physical properties of materials.

2.2 Mixture proportions and mixing procedure

Following ACI guidelines and using the weight method, a fixed w/b ratio of 0.17 was maintained. Ramakrishnan et al. [31] confirmed that a 50 wt% cement replacement with SCMs, such as GGBFS, ensures excellent mechanical and durability properties; thus, GGBFS was replaced at 50 wt%. The binder consisted of cement and GGBFS. Based on the optimization suggested by Xu et al. [32], SF was used to replace silica sand at 10 wt% to improve long-term hydration. The SP dosage was fixed at 1.7% by weight of the binder. The study investigated varying B/S ratios (0.8, 0.9, 1.0, and 1.2) and the incorporation of 6 mm POMF (0 and 2 vol%). Specimens were cast in dimensions of 50 mm × 50 mm × 50 mm and Φ 100 mm × 200 mm. Three replicates were cast for each test and age, with testing conducted at 3, 7, 28, 56, 91, 120, and 180 days. A 50 L large-capacity mixer was employed.

The mixing procedure, illustrated in Figure 2, was as follows:

Dry mixing: All dry powders (cement, GGBFS, SF, and silica sand) were mixed at low speed for 5 min to ensure homogeneity and prevent agglomeration.

Wet mixing (Stage 1): 50% of the total mixing water was added, followed by low-speed mixing for 4 min to moisten the dry materials.

Wet mixing (Stage 2): The remaining 30% of the water was mixed with the total SP dosage. Mixing continued at medium speed for 6 min to form a uniform paste.

Resting: The mixture was allowed to rest for 10 min to allow the SP to react and fully fluidize the paste.

Wet mixing (Stage 3) and fiber addition: Mixing resumed at medium speed for 6 min. POMF was gradually added to the mixer to ensure uniform dispersion within the paste, followed by the addition of the reserved 20% water to assist in fiber dispersion.

Finishing: Upon completion, workability was measured, and specimens were cast. The molds were vibrated on a vibration table for 1 min to expel entrapped air and ensure compaction. They were then covered with plastic film to prevent moisture evaporation (Figure 3). Demolding occurred after 48 h, followed by curing in saturated lime water until the testing age.

Component	SiO_2	Al_2O_3	Fe_2O_3	CaO	MgO	SO_3	LOI	Na_2O	K_2O
Cement	21.4	5.3	3.17	63.5	2.0	2.88	1.4	0.12	0.52
GGBFS	34.4	14.8	0.41	41.7	6.6	0.12	−0.1	0.28	0.37
SF	90	—	—	—	—	—	3.0	—	—
Silica sand	99.5	—	—	—	—	—	—	—	—

Table 1. Chemical compositions of materials (wt%).

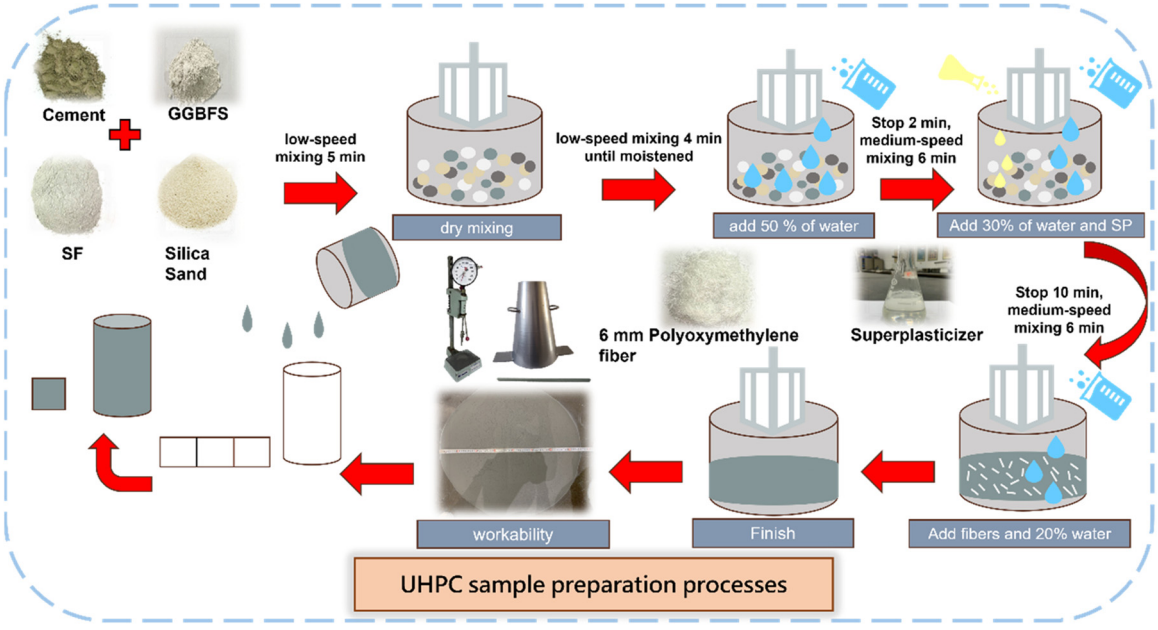


Figure 2. UHPC mixing process.

2.3 Test procedures

2.3.1 Workability

Slump flow is a practical indicator for assessing workability, determining the homogeneity and flowability of concrete under construction conditions. In accordance with ASTM C1611, the slump cone was lifted, and the maximum diameter of the spread circle was measured. The average of four measurements was recorded. Slump flow was remeasured at 0, 30, 60, 90, and 120 min to ensure workability retention, with 1 min of agitation before each measurement.

2.3.2 Mechanical properties

Compressive strength: Tested in accordance with ASTM C109 using 50 mm × 50 mm × 50 mm cubic specimens. A

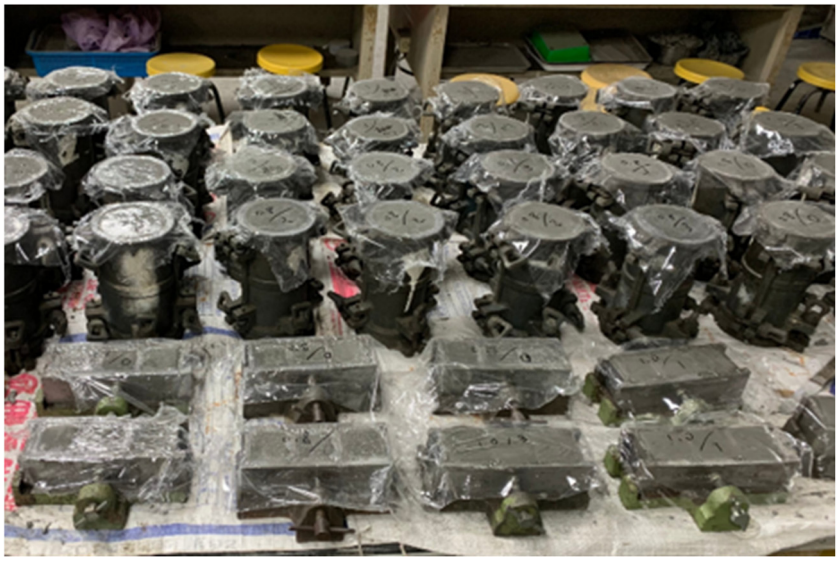


Figure 3. The test specimen was covered with cling film after filling.



Figure 4. Surface resistivity measurement.

150 ton automatic compression testing machine applied an axial load at a rate of 900 kgf/cm^2/min.

Splitting tensile strength: Tested in accordance with ASTM C496 using Φ 100 mm × 200 mm cylindrical specimens. The specimens were secured in a splitting jig and subjected to diametral compression by a 150 ton automatic machine at a loading rate of 10.8 kgf/cm^2/min.

2.3.3 Durability properties

Water absorption: Conducted on 50 mm × 50 mm × 50 mm cubic specimens following ASTM C642. Specimens were oven-dried at 100 ± 5°C for 24 h, cooled to 20–25°C, weighed, immersed in water for 24 h, and then surface-dried and weighed to determine the saturated surface dry (SSD) mass.

Surface resistivity: Measured using a Proceq Resipod concrete resistivity meter in accordance with AASHTO T358 (Figure 4). Measurements were taken on Φ 100 mm × 200 mm cylindrical specimens in the SSD condition to assess matrix density and chloride ion penetration resistance (range: 0–1,000 kΩ cm). The evaluation criteria are presented in Table 3.

Rapid chloride permeability test (RCPT): Conducted according to ASTM C1202 to determine the electrical conductance of concrete, providing a rapid indication of its resistance to chloride ion penetration. Φ 100 mm × 50 mm specimens (Figure 5) were coated with epoxy on the curved surface, vacuum saturated, and placed between two cells containing 3.0% NaCl and 0.3 N NaOH solutions (Figure 6). A 60 V DC potential was applied for 6 h, and the total charge passed (Coulombs) was recorded. The evaluation criteria are presented in Table 4.

Sulfate attack resistance: Conducted in accordance with ASTM C1012. 50 mm × 50 mm × 50 mm cubic specimens were oven-dried, weighed, and immersed in a saturated sodium sulfate (Na_2SO_4) solution. At specified ages, specimens were dried, weighed to calculate weight loss,

Chloride ion penetration	Surface resistivity (kΩ cm)
High	<12
Moderate	12–21
Low	21–37
Very low	37–254
Negligible	>254

Table 3. AASHTO T358 surface resistivity of concrete testing.

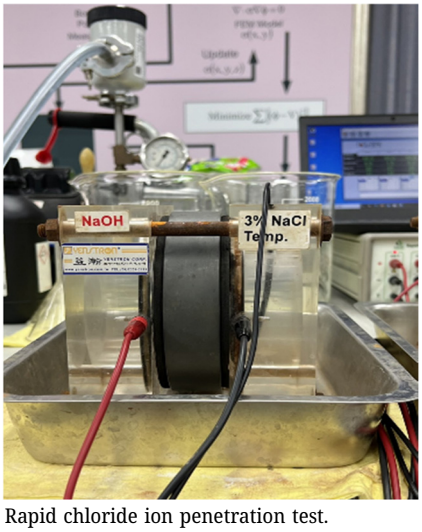


Figure 6. Rapid chloride ion penetration test.

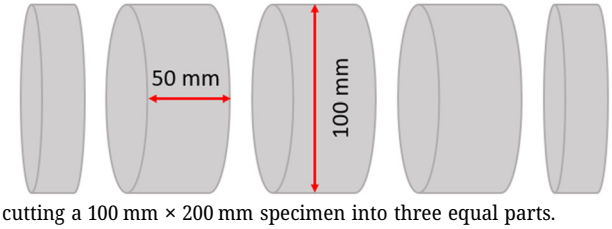


Figure 5. Schematic diagram of cutting a 100 mm × 200 mm specimen into three equal parts.

Charge passed (C)	Chloride ion penetration
>4,000	High
2,000–4,000	Moderate
1,000–2,000	Low
100–1,000	Very low
<100	Negligible

Table 4. ASTM C1202 chloride ion penetrability based on charge passed.

inspected for visual changes, and tested for compressive strength.

2.3.4 Microstructural properties

Microstructural analysis was performed using a field emission SEM. Specimens were crushed and small fragments were immersed in absolute ethanol to arrest hydration, dried, mounted on copper stubs with conductive carbon tape, gold-coated, and observed under SEM to examine microstructures and hydration products.

3. Results and discussion

3.1 Workability

At 0 min, the slump flow of UHPC increased with the B/S ratio. As shown in Figure 7 (0% POMF), the slump flow for B/S 0.8 was 503 mm. Increasing the B/S to 0.9, 1.0, and 1.2 resulted in slump flows of 540, 601, and 739 mm, representing increases of 7.3, 19.5, and 46.9%, respectively. This indicates that workability declines as B/S decreases. A lower B/S implies a higher relative proportion of silica sand and SF. Furthermore, Zhang et al. [33] reported that the extremely high specific surface area of SF dramatically increases the matrix's water demand and significantly alters the preferential adsorption of SPs, thereby negatively affecting rheological behavior. Insufficient free water reduces the critical water film thickness surrounding the solid particles, thereby decreasing overall flowability.

As shown in Figure 8, the addition of 2% POMF hurt workability, consistent with most fiber-reinforced concrete studies. However, when compared to the integration of traditional steel fibers discussed by Huang et al. [34], the reduction in flow caused by POMF is considerably more manageable. Steel fibers, due to their high density and rigidity, frequently induce severe "balling effects" and rapid segregation in highly fluid matrices. In contrast, the workability reduction observed with POMF is primarily attributed to the formation of a 3D network structure within the paste, which creates a gentle interlocking effect, consistent with recent findings by Wen et al. [35] on how various fiber types govern the time-dependent rheology and flowability of UHPC. Because POMF has a lower specific gravity (1.41) compared to steel (~7.8), it remains uniformly suspended in the paste without settling.

Regarding slump flow retention, loss increased with time. Higher B/S ratios actively mitigated slump loss. At 120 min, the B/S 0.8 group showed the highest flow loss (38.1–48.9%), whereas the B/S 0.9 and 1.0 groups exhibited much lower loss rates (30.0–35.7%). Because the SP was

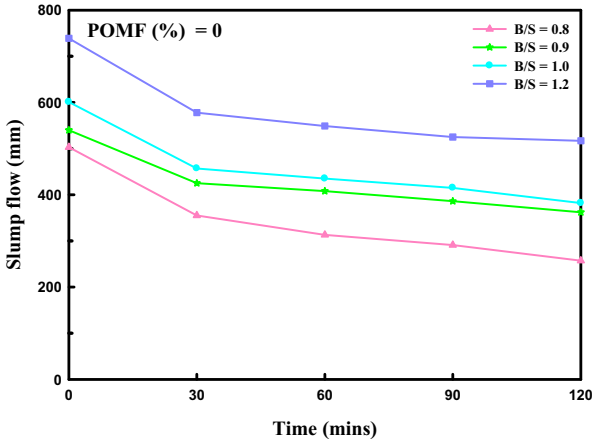


Figure 7. The relationship between slump and time of UHPC with different B/S ratios without adding POMF.

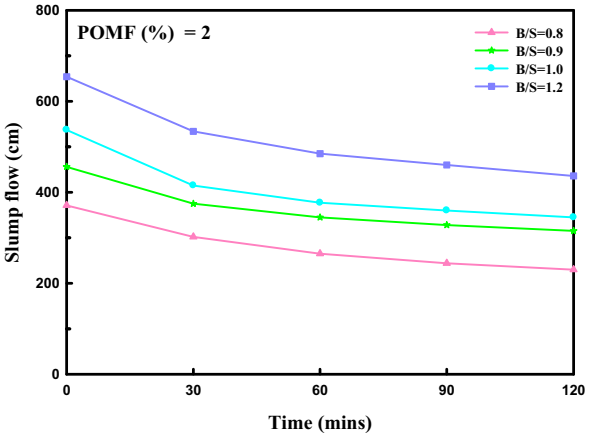


Figure 8. Relationship between slump and time of UHPC with different B/S ratios containing 2% POMF.

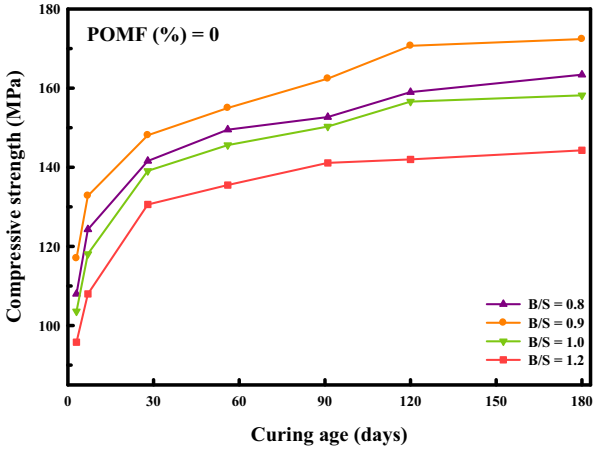


Figure 9. The relationship between compressive strength and age of UHPC with different B/S ratios without adding POMF.

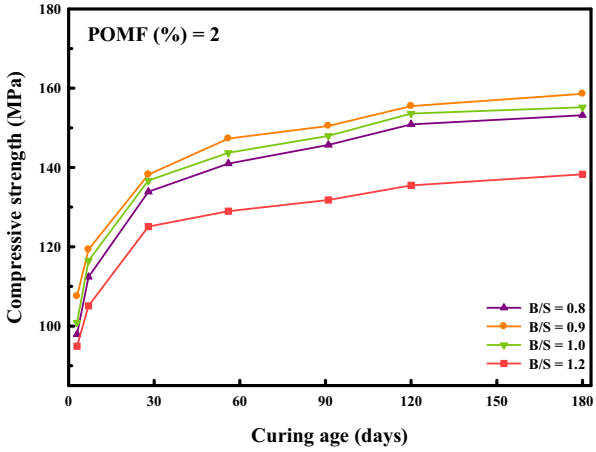


Figure 10. The relationship between compressive strength and age of UHPC with different B/S ratios containing 2% POMF.

fixed at a constant 1.7 wt% of the binder, a higher B/S ratio naturally increased the total absolute amount of liquid SP available in the unit volume of the mix. This excess SP remains in the pore solution, continuously maintaining particle dispersion.

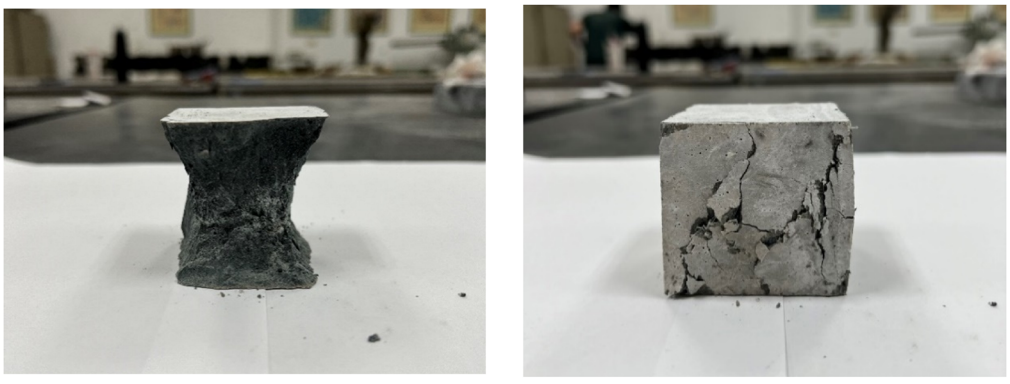
3.2 Mechanical properties

3.2.1 Compressive strength

As shown in Figures 9 and 10, all B/S groups with 0 and 2% POMF achieved exceptional compressive strengths exceeding 120 MPa at 28 days. For the plain UHPC (Figure 9), strength growth was significant before 28 days (26.6–36.3%). Graybeal [36] noted that in ultra-low w/b environments, rapid early hydration forms a rigid skeleton while unhydrated cement and slag particles act as incredibly strong, inert micro-fillers. The late-age strength gain observed up to 180 days is strictly attributed to the latent pozzolanic reaction of the 50% GGBFS. Moula et al. [37] corroborated that this continuous secondary hydration of GGBFS critically refines the microstructural pore network and continually enhances long-term matrix density in eco-friendly UHPC systems. Among the different B/S ratios, the optimal compressive strength was observed at a B/S of 0.9.

B/S 0.8: The high proportion of silica sand resulted in insufficient binder paste to coat the aggregates and fill interstitial voids thoroughly. This lack of paste led to localized macroscopic porosity, structurally weakening the matrix under compressive loads.

B/S > 0.9 (1.0 and 1.2): Interestingly, strength was negatively affected by an over-abundance of binder. Zheng



(a) (b)

Figure 11. Failure mode of compressive test specimen. (a) No POMF added. (b) 2% POMF added.

et al. [38] recently demonstrated that replacing excessive binder with multi-scale solid waste improves ecological efficiency, noting that an overabundance of pure binder exacerbates paste shrinkage without commensurate strength gains. Excessive paste volume at a low w/b ratio results in significant moisture loss, leading to severe autogenous shrinkage and microscopic internal tensions that initiate early failure.

The addition of POMF resulted in only a limited improvement in absolute compressive strength, a finding consistent with those of Rui et al. [27], confirming that compressive strength is primarily governed by matrix density. However, failure mode analysis (Figure 11) revealed that POMF provides a profound lateral confinement effect. Zhang et al. [39] confirmed that while the rigid matrix may crack under peak compression, embedded high-performance polymer fibers bridge these initial defects, sustain the load, and prevent catastrophic explosive failure.

3.2.2 Splitting tensile strength

Splitting tensile strength results (Figures 12 and 13) followed a trend similar to that of compressive strength, peaking at a B/S ratio of 0.9 (exceeding 6 MPa at 28 days). This confirms that optimizing the paste-to-aggregate volume is crucial for tensile stress transfer.

Crucially, fiber addition was the absolutely dominant factor for tensile enhancement. As shown in Figure 13, the addition of 2% POMF increased the 28-day splitting tensile strength of B/S 0.8, 0.9, 1.0, and 1.2 groups by 22.7, 9.5, 11.4, and 23.8%, respectively. This specific range of enhancement aligns closely with Zhang et al. [40], who confirmed

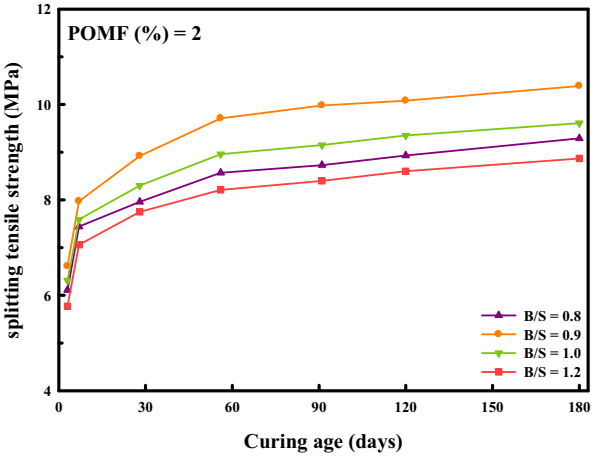


Figure 13. The relationship between splitting strength and age of UHPC with different B/S ratios containing 2% POMF.

via simulations that the hydration products surrounding fibers directly translate to macroscopic tensile bridging. Compared with conventional synthetic fibers, POMF demonstrates a vastly superior structural capacity. The use of 6 mm short fibers facilitated highly uniform 3D distribution and orientation. Figure 14 visually illustrates this exceptionally uniform fiber distribution across the fractured splitting plane.

Notably, the percentage increase in strength was lower for the structurally sound matrices (B/S 0.9 and 1.0) than for the flawed, weaker ones (B/S 0.8 and 1.2). This critical observation suggests that polymer fibers play a highly active “repairing” role in a highly stressed or inherently porous matrix, stepping in to carry loads where the concrete skeleton fails. Failure mode analysis (Figure 15)

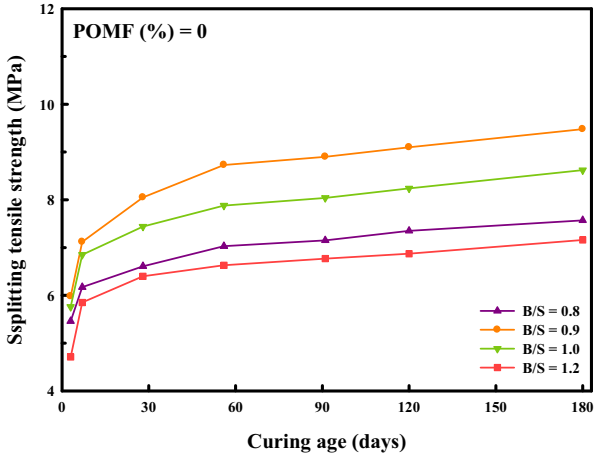


Figure 12. The relationship between splitting strength and aging of UHPC with different B/S ratios without adding POMF.



(a) (b)

Figure 14. Splitting specimen profiles of different POMFs. (a) No POMF added. (b) 2% POMF added.

demonstrated that POMF successfully shifted the ultimate failure from a sudden, dangerous brittle fracture to a cohesive, ductile separation.

3.3 Durability properties

3.3.1 Absorption

As shown in Figures 16 and 17, water absorption for all evaluated groups was strictly maintained below 2%. Anunike et al. [41] emphasized that achieving such an intrinsically dense microstructure is the primary reason UHPC exhibits superior impermeability and durability, even qualifying it for extreme applications such as radiation shielding. Across all groups, absorption decreased progressively with age, driven by microstructural densification from ongoing hydration and pozzolanic reactions. When evaluating different B/S ratios, water absorption reached an absolute minimum at 0.9.

B/S 0.8: Higher absorption than B/S 0.9 was observed due to a physically weaker ITZ. The high sand volume created localized zones completely devoid of cement paste, leaving macro-pores open to water ingress.

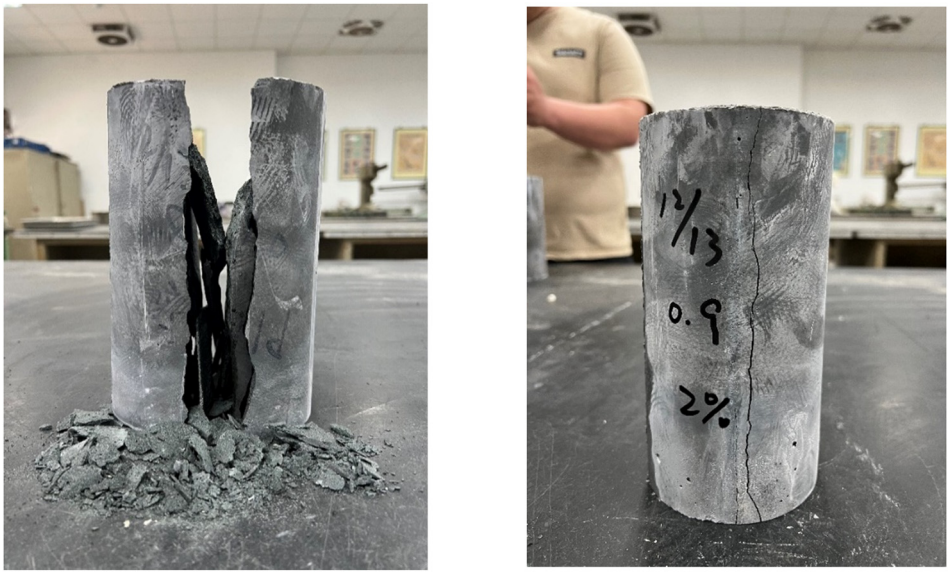
B/S 1.2: Paradoxically, despite having the most binder, absorption increased significantly. Tanimura and Sato [42] demonstrated that excessive unhydrated cement paste leads to immense internal stress and severe autogenous shrinkage during early curing. These shrinkage forces induce a network of microcracks that essentially serve as interconnected capillary pathways for external moisture.

Adding 2% POMF slightly increased water absorption across all groups. This minor negative side effect is commonly attributed to the physical introduction of entrapped micro-voids during the rigorous fiber mixing process.

3.3.2 Surface resistivity

Surface resistivity serves as an excellent, non-destructive, indirect measure of concrete compactness and tortuosity. As expected, resistivity increased linearly with age (Figures 18 and 19). Fonseka and Nanayakkara [43] directly linked this prolonged increase to the continuous formation of secondary C–S–H gel products that actively refine and block the capillary pore structure.

At 28 days, the B/S 0.8, 0.9, and 1.0 groups successfully achieved the highly coveted “Negligible” chloride ion penetration class (>254 kΩ cm) as defined in Table 3. The B/S 1.0 group (without fibers) exhibited the highest absolute resistivity. However, the B/S 1.2 group showed a sudden and noticeable decline in electrical resistance. Ou et al. [44] recently demonstrated, in their long-term microstructural assessments, that continuous hydration of abundant unhydrated particles within UHPC can induce complex internal stresses and structural fluctuations over



(a) (b)

Figure 15. The failure modes of different POMF splitting specimens. (a) No POMF added. (b) 2% POMF added.

time. This phenomenon perfectly explains why the B/S 1.2 mix, which contains a massive excess of unreacted binder, ultimately developed shrinkage-induced microcracks that act as highly conductive fluid channels for ionic transport, thereby severely reducing its electrical resistivity.

Interestingly, adding 2% POMF decreased resistivity in the near-perfect B/S 1.0 matrix (by physically disrupting the otherwise flawless homogeneity), but increased it in the inherently flawed matrices of B/S 0.8 and 1.2. Because POMF is an electrically insulating synthetic polymer, it can strategically interrupt continuous conductive pore networks and physically block ionic pathways when appropriately dispersed in a cracked matrix.

3.3.3 RCPT

Table 5 explicitly details that the total charge passed for all evaluated UHPC groups was extremely low (<100 C). According to the stringent criteria in Table 4, the material is designated as having “Negligible” chloride penetrability.

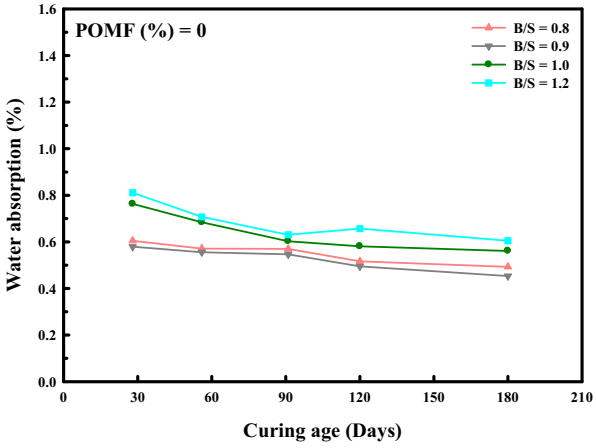


Figure 16. The relationship between water absorption and aging of UHPC with different B/S ratios without adding POMF.

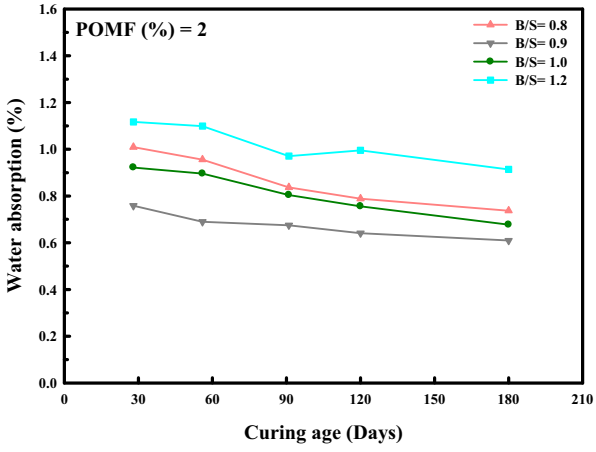


Figure 17. The relationship between water absorption and aging of UHPC with different B/S ratios containing 2% POMF.

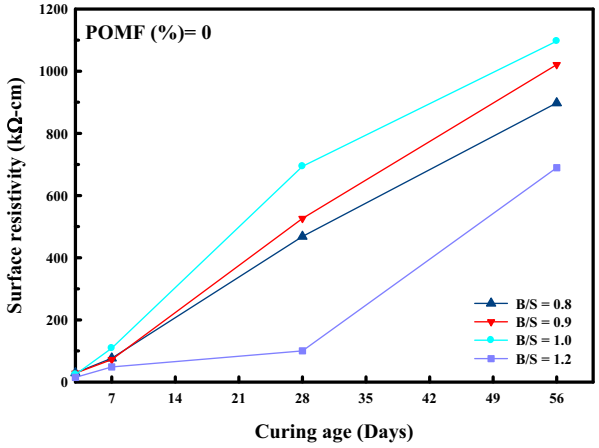


Figure 18. The relationship between surface resistivity and age of UHPC with different B/S ratios without adding POMF.

Turgeon-Malette et al. [45] investigated the chloride ion permeability of ultra-high performance fiber-reinforced concrete under sustained loads, demonstrating that its inherently dense matrix maintains exceptional resistance to chloride ion ingress even when microcracked. This finding provides crucial support for our RCPT results, in which the highly synergistic use of 50% GGBFS replacement and SF filling physically blocks chloride pathways, enabling all evaluated UHPC groups to achieve extremely low sub-100 C values associated with "Negligible" penetrability. While the macroscopic variations were minor, the B/S 1.2 mix showed slightly higher charge passage than the

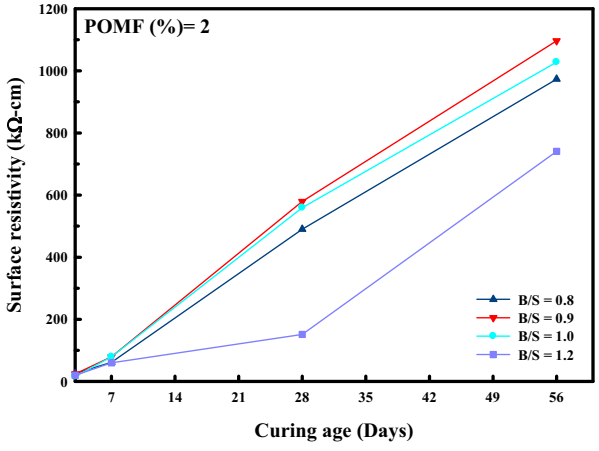


Figure 19. The relationship between surface resistivity and age of UHPC with different B/S ratios containing 2% POMF.

Age (days)	0.8P0	0.9P0	1.0P0	1.2P0	0.8P2	0.9P2	1.0P2	1.2P2
28	26	23	28	40	29	19	24	32
56	19	15	21	31	23	13	17	28
91	15	11	17	27	19	10	12	23
120	12	10	14	25	17	8	10	22
180	11	8	12	21	13	6	8	17

Unit: Coulomb, P: POMF.
Table 5. Chloride ion penetrability based on charge passed test.

Age (days)	0.8P0	0.9P0	1.0P0	1.2P0	0.8P2	0.9P2	1.0P2	1.2P2
28	−046	−0.21	−0.71	−2.63	−0.70	−0.31	−0.71	−1.12
56	−0.66	−0.60	−1.20	−0.88	−0.90	−0.77	−1.20	−0.66
91	−0.87	−0.51	−0.58	−0.96	−0.73	−0.65	−0.58	−0.69
120	−0.75	−0.65	−0.61	−0.85	−0.53	−0.90	−0.61	−0.67
180	−0.69	−0.86	−0.67	−0.81	−0.46	−1.07	−0.67	−0.58

Unit: %, P: POMF.
Table 6. Sulfate weight loss rate.

B/S 0.9 mix, perfectly corroborating the detrimental water absorption and resistivity degradation results discussed previously. The addition of POMF did not significantly compromise this elite level of impermeability, demonstrating its safety for marine applications.

3.3.4 Sulfate attack resistance

Table 6 indicates that specimens immersed in a highly aggressive Na_2SO_4 solution initially gained mass (recorded as a negative weight loss). Zhang et al. [46] reported similar initial weight gains in extremely dense concrete systems. In these early stages, sulfate crystallization occurs safely within the pre-existing surface pores, actually densifying the outer layer temporarily without causing immediate internal expansion. Specimens containing 2% POMF exhibited slightly greater weight variations. Gu et al. [47] noted that flexible synthetic fibers can subtly modify micro-pore connectivity, potentially creating localized, harmless zones for early crystallization. Remarkably, Figure 20 shows absolutely no visible spalling, corner degradation, or surface cracking even after 180 days of continuous full immersion. Pham [48] conducted a comprehensive state-of-the-art review of fiber-reinforced concrete, confirming that synthetic polymer fibers inherently exhibit high chemical stability in both high-alkaline cement environments and external sulfate environments, thereby preventing long-term fiber decomposition.

The compressive strength tests (Figures 21 and 22) conducted during the sulfate immersion revealed critical, long-term divergent behaviors based on the B/S ratio:

B/S 0.8: Strength initially increased due to pore-filling, but then declined sharply at later ages. This indicates that the inherently porous nature of the low-paste matrix eventually permitted deep sulfate ingress, ultimately succumbing to overwhelming expansive internal pressures from delayed ettringite formation.

B/S 0.9: Showed virtually zero strength decline. Impressively, it exhibited continued strength growth up to 180 days. This confirms that its structurally optimized, dense ITZ completely blocked sulfate ion penetration, protecting the internal C–S–H bonds.

B/S 1.0 and 1.2: Exhibited a steady, progressive strength decline over time. While physically dense, the higher absolute paste volume intrinsically provided substantially more vulnerable chemical reactants – specifically calcium aluminate phases and residual CH – for the sulfate ions to attack.

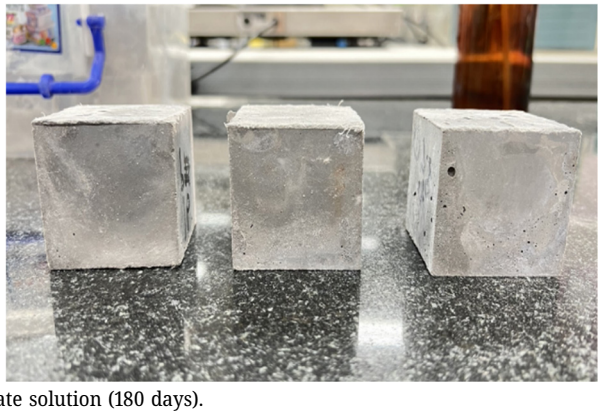


Figure 20. Sample soaked in sulfate solution (180 days).

3.4 Microstructural properties

The microstructural characteristics of UHPC exert a direct and profound influence on its macroscopic mechanical properties and long-term durability. Using SEM, the morphological evolution of hydration products and the ITZ were systematically evaluated at different curing ages.

As illustrated in Figure 23a, at an early curing age of 3 days, the microstructure is predominantly characterized by an abundance of short, needle-like structures. These acicular formations are identified as a complex mixture of early-stage calcium silicate hydrate (C–S–H) gels, initial calcium hydroxide (CH) crystals, and ettringite. The rapid precipitation of these specific formations is driven by the highly accelerated early hydration kinetics typical of UHPC mixtures formulated with a low water-to-binder ratio and potent SPs, a mechanism documented by Chen et al. [49]. This rapid initial reaction constructs a rigid primary framework, but it remains highly heterogeneous.

As the curing period extends to 7 days (Figure 23b), a distinct morphological transformation within the cementitious matrix becomes evident. The previously dominant short, needle-like ettringite and initial hydration structures noticeably diminish in quantity. In their place, a massive volume of relatively loose, amorphous C–S–H gel begins to dominate the matrix, accompanied by the appearance of scattered plate-like CH crystals, consistent with the dense matrix developments analyzed by Yazıcı et al. [50]. By the 28-day mark (Figure 23c), the primary hydration reactions are fundamentally complete. The overall microstructural architecture transitions into a highly dense, compact, and homogeneous state.

The long-term microstructural stability was evaluated at the 56 and 91-day marks (Figure 23d). At these advanced

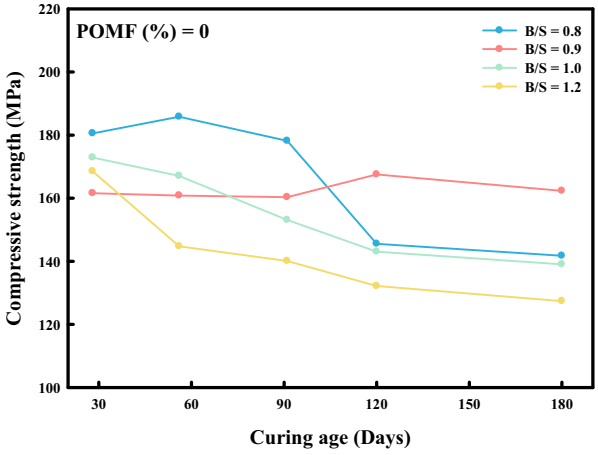


Figure 21. The relationship between the age and compressive strength of UHPC with different B/S ratios without adding POMF.

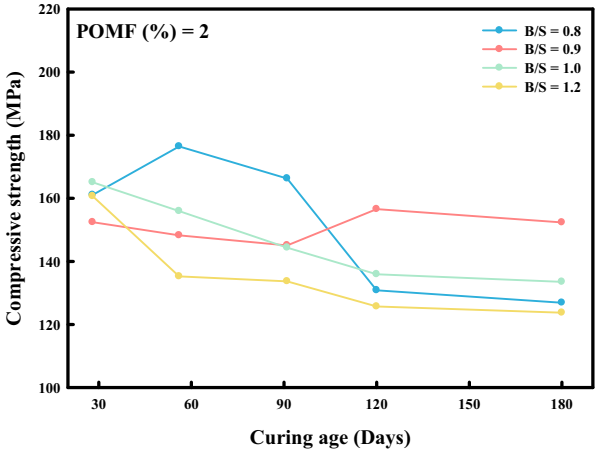


Figure 22. The relationship between UHPC aging and compressive strength with 2% POMF for different B/S ratios.

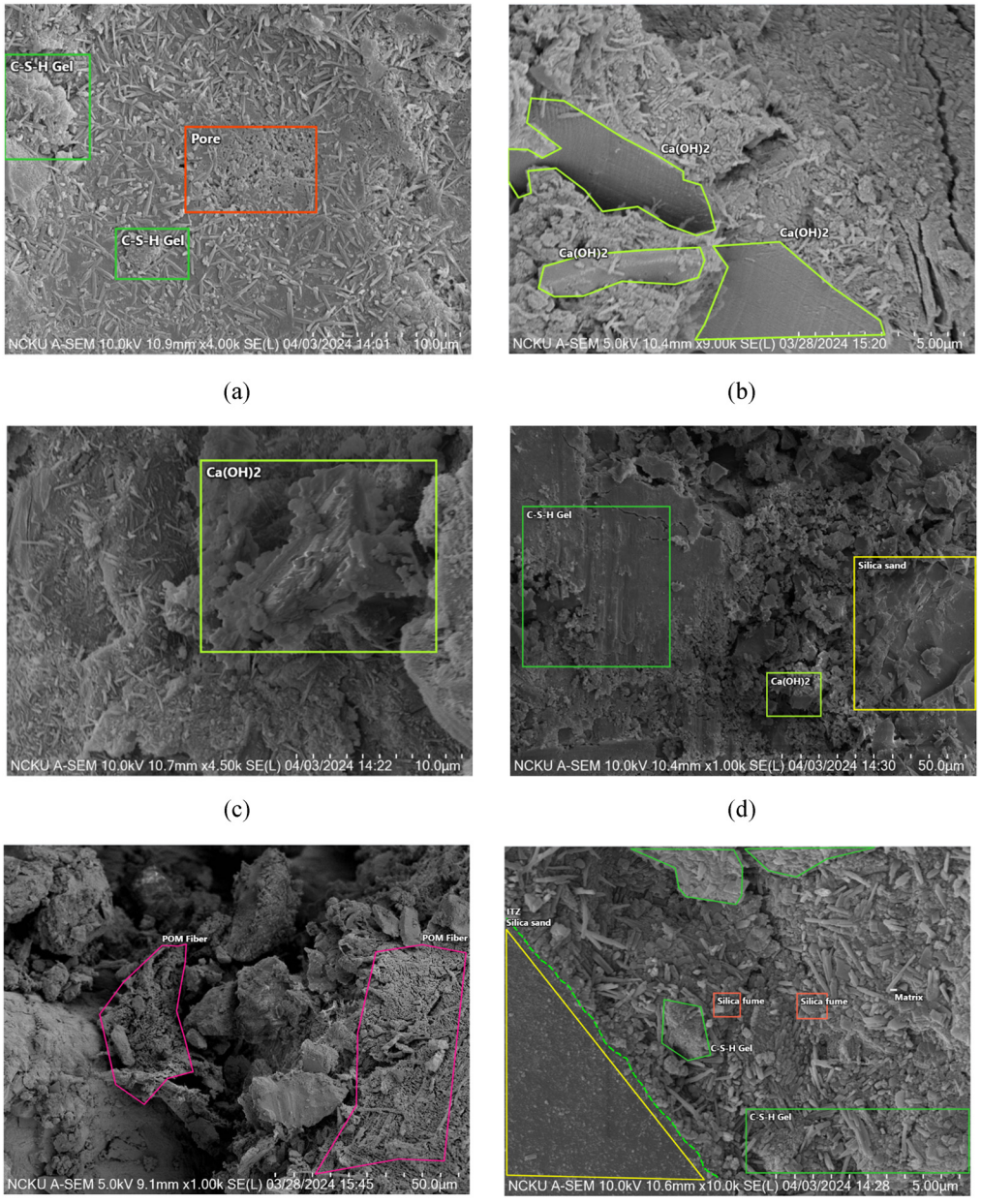


Figure 23. SEM image of UHPC. (a) SEM at 3 days of age. (b) SEM at 7 days of age. (c) SEM at 28 days of age. (d) SEM at 56 days of age. (e) Adhesive properties between POMF and substrate. (f) ITZ of silica sand and substrate.

stages, the C–S–H gel within the matrix presents an extraordinarily high degree of crystallinity. A critical observation during these later ages is the virtual disappearance of distinct, large CH crystals. This phenomenon is a direct macroscopic result of the intense secondary pozzolanic reactions facilitated by the 50% replacement of GGBFS and the 10% SF.

Beyond the bulk matrix hydration, the interaction between the novel POMFs) and the surrounding cementitious paste is a critical determinant of the composite's ductility. As clearly depicted in the 28-day SEM micrograph focusing on the fiber interface (Figure 23e), there is an exceptionally high quality of adhesive bonding between the POMF and the surrounding substrate. This superior

interfacial adhesion is primarily due to the POMF's inherent hydrophilic nature. Instead of a smooth, debonded interface typical of many synthetic fibers, the POMF is tightly wrapped and physically interlocked by the hydration products.

Finally, the structural integrity of the ITZ between the inert aggregates and the reactive paste was examined. As shown in Figure 23f, the interface between the fine silica sand particles and the UHPC matrix exhibits a remarkably dense, tight, and continuous bond. There are no obvious microcracks, porous zones, or significant gaps, which typically characterize the ITZ in conventional concrete. This seamless integration confirms that the optimized B/S ratio of 0.9 provides precisely the adequate volume of paste required to fully envelop the aggregate particles without inducing excessive autogenous shrinkage.

3.5 Overall evaluation and practical implications

The comprehensive evaluation of fresh, mechanical, and durability properties explicitly highlights the profound architectural and environmental effects of optimizing the B/S ratio and incorporating POMF.

Advantages: The precisely optimized B/S 0.9 mixture, combined with an aggressive 50% GGBFS replacement strategy, offers an exceptionally eco-efficient and highly durable UHPC solution. The strategic addition of 2% POMF significantly enhances the material's structural ductility, effectively altering its failure mode from a catastrophic brittle fracture to a safer, cohesive, energy-absorbing response. Furthermore, this specific composite formulation exhibits outstanding resistance to chloride ion penetration (<100 C) and absolute integrity against long-term sulfate attack. As corroborated by Lin et al. [28] in their extensive economic assessment, using synthetic polymeric fibers such as POMF instead of traditional steel fibers drastically reduces the overall structural dead load and effectively eliminates the risk of fiber surface corrosion.

Limitations and drawbacks: The primary physical limitation observed in this study is the notable reduction in initial workability and an accelerated slump loss. This is an unavoidable consequence of the POMF's massive surface area and internal 3D networking. Additionally, the data unequivocally shows that deviating from the optimal B/S ratio – particularly by operating under the false assumption that an excessive binder content (B/S 1.2) is superior – poses a critical engineering risk. This overdesign causes severe autogenous shrinkage and subsequent internal microcracking, which severely compromises long-term chemical durability.

Practical Benefits: In practical, real-world field applications, this optimized, slag-blended, POMF-reinforced UHPC provides a highly cost-effective, low-carbon alternative to traditional, cement-heavy, steel-reinforced UHPC mixtures. Its superior post-cracking tensile strength, combined with an almost impenetrable matrix, makes it highly suitable for manufacturing slender, lightweight precast elements deployed in highly aggressive environments. It is exceptionally well-suited for critical infrastructure such as marine seawalls, high-traffic bridge decks, and chemical storage facilities, where both sustained structural toughness and a drastically extended service life are paramount requirements.

4. Conclusion

This study investigated the engineering properties of UHPC with a fixed w/b of 0.17, varying B/S ratios (0.8, 0.9, 1.0, and 1.2), and POMF dosages (0 and 2%). The following conclusions are drawn:

(1) B/S ratio as a critical parameter: The B/S ratio is a decisive factor governing UHPC performance. A B/S ratio of 0.9 was identified as the optimal equilibrium point, achieving the best balance between 28-day compressive strength, splitting tensile strength, water absorption, and chemical sulfate resistance.

(2) Optimization over maximization: Higher binder content is not synonymous with better performance. Excessive binder (B/S 1.2) acts detrimentally, inducing severe autogenous shrinkage and microcracking that compromise overall durability. Conversely, insufficient binder (B/S 0.8) leads to poor aggregate coating and high porosity.

(3) Fiber reinforcement efficiency: The addition of 2% POMF provided limited compressive gains but significantly enhanced splitting tensile strength. Notably, the reinforcement efficiency was disproportionately higher in structurally weaker or flawed matrices (e.g., a ~23% increase in B/S 0.8 and 1.2 mixes) compared to optimized matrices (a ~10% increase in B/S 0.9 and 1.0 mixes), demonstrating the fibers' capacity to bridge intrinsic micro-defects.

(4) Future work: Further research should build upon the optimal B/S 0.9 mix to explore the synergistic effects of hybrid fiber systems (e.g., steel-POMF blends) and to conduct long-term impact resistance testing. Standardized autogenous shrinkage measurements (ASTM C1698) are also highly recommended for future validation.

Funding information

Authors state no funding involved.

Author contributions

Wen-Ten Kuo: resources, conceptualization, investigation, writing – original draft, writing – review and editing. Wen-Ling Wang: resources, data curation, investigation, writing – original draft. Sung-Ching Chen: resources, methodology, formal analysis, visualization, supervision, validation, writing – review and editing.

Conflict of interest statement

Authors state no conflict of interest.

Data availability statement

The data used to support the findings of this study are available from the corresponding author upon request.

References

[1] Bajaber, M.A., Hakeem, I.Y., UHPC evolution, development, and utilization in construction: A review, J. Mater. Res. Technol., 2021; 10: 1058

[2] Yoo, D.-Y., Banthia, N., Mechanical properties of ultra-high-performance fiber-reinforced concrete: A review, Cem. Concr. Compos., 2016; 73: 267

[3] Xu, D., Tang, J., Hu, X., Yu, C., Han, F., Sun, S., et al., The influence of curing regimes on hydration, microstructure and compressive strength of ultra-high performance concrete: A review, J. Build. Eng., 2023; 76: 107401

[4] Yoo, D.-Y., Oh, T., Banthia, N., Nanomaterials in ultra-high-performance concrete (UHPC) – A review, Cem. Concr. Compos., 2022; 134: 104730

[5] Shi, C., Wu, Z., Xiao, J., Wang, D., Huang, Z., Fang, Z., Genetic and biochemical mechanisms of pollen wall development, Constr. Build. Mater., 2015; 101: 741

[6] Ghafari, E., Costa, H., Júlio, E., Statistical mixture design approach for eco-efficient UHPC, Cem. Concr. Compos., 2015; 55: 17

[7] Yu, R., Spiesz, P., Brouwers, H.J.H., Mix design and properties assessment of ultra-high performance fibre reinforced concrete (UHPFRC, Cem. Concr. Res., 2014; 56: 29

[8] Sharma, R., Jang, J.G., Bansal, P.P., A comprehensive review on effects of mineral admixtures and fibers on engineering properties of ultra-high-performance concrete, J. Build. Eng., 2022; 45: 103314

[9] Song, J., Banthia, N., Yoo, D.-Y., Effect of supplementary cementitious materials on durability of ultra-high-performance concrete: A review, Cem. Concr. Compos., 2025; 163: 106198

[10] Khan, I., Yong, G., Role of supplementary cementiteous materials in mitigating heat of hydration in mass concrete elements, Constr. Build. Mater., 2024; 431: 136482

[11] Bellum, R.R., Muniraj, K., Madduru, S.R.C., Exploration of mechanical and durability characteristics of fly ash-GGBFS based green geopolymer concrete, SN Appl. Sci., 2020; 2: 919

[12] Zaki, A., Kusumawijaya, A.M., Rosyidi, S.A.P., Abdullah, M.Z., Mahbubi, K., Ibrahim, Z., Non-destructive based performance analysis of eco-friendly concrete mixes against corrosion and structural degradation, Structures, 2025; 81: 110233

[13] Zhang, Z., Ahmad, N., Shrestha, A., Tang, Z., Cai, Z., Ergashev, R., et al., Investigation of fresh, shrinkage, and mechanical properties in iron sand high-strength engineered cementitious composites: Effects of water-to-binder ratio and fiber volume fraction, Case Stud. Constr. Mater., 2025; 22: e04138

[14] Kim, H., Koh, T., Pyo, S., Enhancing flowability and sustainability of ultra high performance concrete incorporating high replacement levels of industrial slags, Constr. Build. Mater., 2016; 123: 153

[15] Wei, X., Zhu, H., Chen, Q., Ju, J.W., Cai, W., Yan, Z., et al., Microstructure-based prediction of UHPC's tensile behavior considering the effects of interface bonding, matrix spalling and fiber distribution, Cem. Concr. Compos., 2023; 139: 105015

[16] Wang, Y., Qiao, P., Sun, J., Chen, A., Influence of fibers on tensile behavior of ultra-high performance concrete: A review, Constr. Build. Mater., 2024; 430; 136432

[17] Yao, Z., Xu, T., Dong, M., Huang, H., Zeng, Q., Xu, H., et al., Engineered cementitious composites with 100% coral sand aggregate: Effect of water-to-binder and sand-to-binder ratios on mechanical properties and cracking behavior, J. Build. Eng., 2025; 115: 114589

[18] Zailani, W.W., Apandi, N.M., Adesina, A., Alengaram, U.J., Faris, M.A., Tahir, M.F., Physico-mechanical properties of geopolymer mortars for

repair applications: Impact of binder to sand ratio, Constr. Build. Mater., 2024; 412: 134721
[19] Paul, A., John, E., Study on the optimisation of cement and binder content to develop a sustainable high-performance concrete, Mater. Today: Proc., 2023. In Press, doi: 10.1016/j.matpr.2023.12.012
[20] Wahab, S., Abbasi, A.M., Ahmed, A., Khan, I.U., Influence of acetic acid treated recycled concrete aggregates on the rheological and mechanical properties of self-compacting concrete: Experiments and machine learning, Constr. Build. Mater., 2025; 491: 142770
[21] Zhao, S., Liu, R., Liu, J., Yang, L., Comparative study on the effect of steel and plastic synthetic fibers on the dynamic compression properties and microstructure of ultra-high-performance concrete (UHPC), Compos. Struct., 2023; 324: 117570
[22] Shen, D., Liu, C., Luo, Y., Shao, H., Zhou, X., Bai, S., Early-age autogenous shrinkage, tensile creep, and restrained cracking behavior of ultra-high-performance concrete incorporating polypropylene fibers, Cem. Concr. Compos., 2023; 138: 104948
[23] Pakravan, H.R., Ozbakkaloglu, T., Synthetic fibers for cementitious composites: A critical and in-depth review of recent advances, Constr. Build. Mater., 2019; 207: 491
[24] Deng, Z., Chen, P., Liu, X., Du, L., Tan, J., Liang, N., Study on the tensile and compressive mechanical properties of multi-scale fiber-reinforced concrete: Laboratory test and mesoscopic numerical simulation, J. Build. Eng., 2024; 86: 108852
[25] Shen, C., Tang, D., Lyu, Z., Yang, C., Yu, L., Distribution of coarse aggregate and steel fibers in ultra-high performance concrete containing coarse aggregate (UHPC-CA) and their effect on the flexural performance, Constr. Build. Mater., 2024; 421: 135666
[26] Zhang, W., Xu, X., Wang, H., Wei, F., Zhang, Y., Experimental and numerical analysis of interfacial bonding strength of polyoxymethylene reinforced cement composites, Constr. Build. Mater., 2019: 207: 1
[27] Rui, Y., Li, K., Yang, T., Tang, L., Dong, M., Shi, Z., Comparative study on the effect of steel and polyoxymethylene fibers on the characteristics of ultra-high performance concrete (UHPC), Cem. Concr. Compos., 2022; 127: 104418
[28] Lin, J.-X., Luo, R.-H., Su, J.-Y., Guo, Y.-C., Chen, W.-S., Coarse synthetic fibers (PP and POM) as a replacement to steel fibers in UHPC: Tensile behavior, environmental and economic assessment, Constr. Build. Mater., 2024; 412: 134654
[29] Shen, D., Shao, H., Huang, Y., Liu, C., Huang, Q., Zhao, C., Influence of polyoxymethylene fibers on autogenous shrinkage, tensile creep, and cracking resistance of ultra-high performance concrete, Cem. Concr. Compos., 2025; 154: 105766.
[30] ACI Committee 239, Ultra-high-performance concrete: An emerging technology report (ACI 239R-18), American Concrete Institute, Farmington Hills, 2018
[31] Ramakrishnan, K., Pugazhmani, G., Sripragadeesh, R., Muthu, D., Venkatasubramani, C., Experimental study on the mechanical and durability properties of concrete with waste glass powder and ground granulated blast furnace slag as supplementary cementitious materials, Constr. Build. Mater., 2017; 156: 739
[32] Xu, D., Tang, J., Hu, X., Zhou, Y., Yu, C., Han, F., et al., Influence of silica fume and thermal curing on long-term hydration, microstructure and compressive strength of ultra-high performance concrete (UHPC), Constr. Build. Mater., 2023; 395: 132370
[33] Zhang, Q., Shu, X., Yang, Y., Wang, X., Liu, J., Ran, Q., Preferential adsorption of superplasticizer on cement/silica fume and its effect on rheological properties of UHPC, Constr. Build. Mater., 2022; 359: 129519
[34] Huang, H., Gao, X., Khayat, K.H., Su, A., Influence of fiber alignment and length on flexural properties of UHPC, Constr. Build. Mater., 2021; 290: 122863
[35] Wen, K.-W., Su, Y.-F., Mo, K.H., Hung, C.-C., Time-dependent rheology, green strength, and buildability of 3D-printed ultra-high performance concrete incorporating various fiber types and contents, J. Build. Eng., 2026; 117: 114919
[36] Graybeal, B.A., The performance of ultra-high performance concrete, US Department of Transportation, Federal Highway Administration, Washington, DC, 2014
[37] Moula, S., Fraj, A.B., Trauchessec, R., Wattez, T., Bouasker, M., Ali, N.B.H., New approach for developing an eco-friendly ultra-high performance concrete making efficient use of ground granulated blast-furnace slag, Constr. Build. Mater., 2025; 503: 144512
[38] Zheng, Z., Tan, H., Zeng, J., Yang, J., Zheng, G., Zhu, M., et al., Ecological ultra-high performance concrete incorporating multi-scale and multi-source solid wastes as nano-micron filler, ultrafine binder and fine aggregate, Constr. Build. Mater., 2025; 463: 140002
[39] Zhang, J.C., Li, B.J., Chen, W.Y., Guo, R.X., Experimental investigations on tensile strength and fracture toughness of a polyoxymethylene fiber reinforced concrete, Theor. Appl. Fract. Mech., 2024; 130: 104250
[40] Zhang, G., Zhang, W., Li, Y., Chen, H., Ge, J., Pan, P., et al., The effect of curing regimes on the hydration

products of lightweight ultra-high performance concrete: From experiments to MD simulations, Constr. Build. Mater., 2024; 412: 134865

[41] Anunike, G.S., Tarabin, M., Hisseine, O.A., Assessment of the mechanical, radiation shielding, and durability of ultra-high-performance concrete for radiation shielding: A review, Constr. Build. Mater., 2025; 474: 140896

[42] Tanimura, M., Sato, R., Influence of autogenous shrinkage on the microstructure and permeability of high-strength concrete, Cem. Concr. Res., 2017; 99: 119

[43] Fonseka, N.H.I.C., Nanayakkara, S.M.A., Assessment of Concrete Durability by Surface Resistivity and Initial Surface Absorption in 12th International Conference on Structural Engineering and Construction Management, Springer, Singapore, 2022, p. 603

[44] Ou, Y., Ji, X., Pan, J., Su, A., Gao, X., Sun, M., et al., Long-term performance and microstructure evolution of UHPC with exposure to seawater immersion, J. Build. Eng., 2025; 111: 113640

[45] Turgeon-Malette, V., Chen, X., Bah, A.S., Conciatori, D., Sanchez, T., Teguedy, M.C., et al., Chloride ion permeability of ultra-high-performance fiber-reinforced concrete under sustained load, J. Build. Eng., 2023; 66: 105842

[46] Zhang, H., Ji, T., Liu, H., Performance evolution of recycled aggregate concrete (RAC) exposed to external sulfate attacks under full-soaking and dry-wet cycling conditions, Constr. Build. Mater., 2020; 248: 118675

[47] Gu, Y., Martin, R.-P., Metalssi, O.O., Fen-Chong, T., Dangla, P., Pore size analyses of cement paste exposed to external sulfate attack and delayed ettringite formation, Cem. Concr. Res., 2019; 123: 105766.

[48] Pham, T.M., Fibre-reinforced concrete: State-of-the-art-review on bridging mechanism, mechanical properties, durability, and eco-economic analysis, Case Stud. Constr. Mater., 2025; 22: e04574

[49] Chen, T., Gao, X., Ren, M., Effects of autoclave curing and fly ash on mechanical properties of ultra-high performance concrete, Constr. Build. Mater., 2018; 158: 864

[50] Yazıcı, H., Deniz, E., Baradan, B., The effect of autoclave pressure, temperature and duration time on mechanical properties of reactive powder concrete, Constr. Build. Mater., 2013; 42: 53